Journal of Medicinal Chemistry

ARTICLE

pubs.acs.org/jmc

Inhibition of Myosin ATPase Activity by Halogenated Pseudilins: A Structure−Activity Study

Matthias Preller,[†] Krishna Chinthalapudi,[†] René Martin,[§] Hans-Joachim Knölker,[§] and Dietmar J. Manstein*[,†,‡]

[†]Institute for Biophysical Chemistry, OE4350, and [‡]Research Centre for Structural Analysis, OE8830, Hannover Medical School, 30625 Hannover

[§]Department of Chemistry, Technical University of Dresden, 01069 Dresden

Supporting Information

ABSTRACT: Myosin activity is crucial for many biological functions. Strong links have been established between changes in the activity of specific myosin isoforms and diseases such as cancer, cardiovascular failure, and disorders of sensory organs and the central nervous system. The modulation of specific myosin isoforms therefore holds a strong therapeutic potential. In recent work, we identified members of the marine alkaloid family of pseudilins as potent inhibitors of myosin-dependent processes. Here, we report the crystal structure of the complex between the *Dictyostelium* myosin 2 motor domain and 2,4-dichloro-6-(3,4,5-tribromo-1*H*-pyrrole-2-yl)phenol (**3**). Detailed comparison with previously solved structures of the myosin 2 complex with bound pentabromopseudilin (**2a**) or pentachloropseudilin (**4a**) provides insights into the molecular basis of the allosteric communication between the catalytic and the allosteric sites. Moreover, we describe the inhibitory potency for a congeneric series of halogenated pseudilins. Insight into their mode of action is gained by applying a combination of experimental and computational approaches.

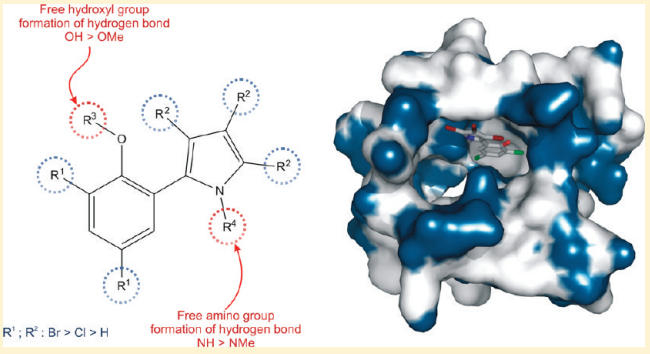

INTRODUCTION

Motile and transport processes in biological systems rely on the activity of molecular motors, such as myosins, kinesins, and dyneins. Members of the superfamily of myosin motors participate in a large number of bioprocesses including cytokinesis, mitosis, chemotaxis, intracellular transport of vesicles and organelles, exocytosis, and endocytosis. The energy for the mechanical work produced by myosin motors is provided by ATP hydrolysis, while actin filaments (F-actin) form the tracks on which the motors walk. The malfunction of certain myosins due to a mutation or an insertion/deletion polymorphism in the gene encoding the myosin heavy chain can lead to severe diseases such as familial hypertrophic cardiomyopathy, deafness, and blindness. Cancer cells and several pathogens rely to an increased extent on myosin motor activity for active spreading, rapid growth, and the penetration of cells and tissues. For this reason, the efficient activation or inhibition of specific myosin motors with the aid of small druglike compounds is of considerable medical relevance. Recently, we discovered and reported the significant inhibitory effect of two members of the marine natural product class of halogenated pseudilins (2-phenylpyrroles) on myosin motor activity.[1,2] Pseudilins were first described as antibiotic products of marine bacteria *Chromobacterium* sp., *Pseudomonas bromoutiliz*, and *Alteromonas luteoviolaceus* and were shown to exhibit antitumor, antimicrobial, and phytotoxic activities. Moreover, they were shown to inhibit human 12- and 15-lipoxygenases and nonspecific liver esterase.[3] Different synthetic routes were applied for the synthesis of pentabromopseudilin (PBP) and related compounds.[3a,4] Here, we used a silver(I)-catalyzed cyclization of homopropargylamines to 2-aryl-substituted pyrroles for the synthesis of our test compounds, as reported earlier.[5]

PBP was shown previously to inhibit myosin 2-dependent processes such as isometric tension development and unloaded shortening velocity in muscle cells. Because of differences in the abundance of myosin isoforms, PBP can also be used in cell biological applications to induce myosin 5-dependent changes, such as altered mitochondrial morphology.[1] Steady-state ATPase measurements in the presence of F-actin and with the use of different myosin isoforms revealed a preference of PBP for class 5 myosins over members of classes 1 and 2. The highest affinity and lowest half-maximal inhibitory concentration (IC_{50}) of around 1.2 μM was observed with chicken myosin 5a. The chlorinated derivative pentachloropseudilin (PClP) displays an entirely different specificity, with the highest inhibitory potency displayed toward class 1 myosins ($IC_{50} \approx 1.0$ μM for *Dd* myosin 1B) and

Received: October 18, 2010
Published: May 02, 2011

an IC_{50} of only around 100 μM for both class 2 and class 5 myosins (see the Supporting Information, Figure 2SI). Crystallographic analysis of the PBP− and PClP−*Dictyostelium discoideum* (*Dd*) myosin 2 complexes revealed a previously unobserved allosteric binding pocket in the myosin motor domain, positioned near actin-binding residues at the tip of the motor domain and at a distance of 16 Å from the nucleotide-binding pocket. Despite the large amount of kinetic, mechanical, and structural data on the inhibition of myosin by both PBP and PClP, the detailed mechanism of how the pseudilins operate on myosin remains elusive. Here, we present structure−activity relationship (SAR) studies on 11 selected pseudilin derivatives. Although the test set is relatively small, the combination of static crystallographic approaches and kinetic experiments together with dynamic computational simulations provides comprehensive insights into the mechanism responsible for the allosteric inhibition of myosin motor activity by halogenated pseudilins. The influence of different substitutions and the importance of hydrogen bond donor and acceptor groups are discussed, as well as entropic contributions to binding and inhibitory activity.

RESULTS

Eleven halogenated pseudilins were selected and subjected to the present SAR analysis. They are closely related but differ in the nature of the substituents at the phenol and pyrrole rings. We used brominated and chlorinated compounds, as well as pseudilins with mixed substitutions for this study. In addition, some compounds are methylated at the hydroxyl group or at the amino group of the pyrrole ring (see Table 1).

Structural Analysis. Crystal structures for the complexes of the *Dd* myosin 2 motor domain with ligands **2a** and **4a** were solved earlier and revealed a novel allosteric binding site in the myosin motor domain (PDB codes: 2JHR and 2XEL).[1,2] The favored allosteric binding pocket for pseudilins is about 16 Å away from the nucleotide-binding pocket and close to the actin-binding region, at the tip of the 50 kDa cleft. The pocket is open to the exterior and to the large cleft that separates the upper 50 kDa and lower 50 kDa domains of the myosin head. Despite the conserved binding site, **2a** and **4a** were found to adopt different conformations and to be engaged in distinct interactions with the protein.

To elucidate the binding mode of the halogenated pseudilins with mixed substitution and to allow a comparison of the binding behavior, we crystallized the ternary complex formed by the *Dd* myosin 2 motor domain, adenosine diphosphate-*meta*-vanadate ($ADP \cdot VO_3$), and 2,4-dichloro-6-(3,4,5-tribromo-1*H*-pyrrole-2-yl)-phenol or tribromodichloropseudilin (TBDClP) (**3**). The X-ray crystal structure of the complex was solved by molecular replacement and refined to a resolution of 2.4 Å (PDB code: 2XO8). The electron density for pseudilin **3** is unambiguous. Compound **3** binds to the same binding site, first observed with PBP (**2a**) and later with PClP (**4a**), but in a way that is clearly different from the previously observed binding patterns. The phenol and pyrrole rings of **3** and **4a** are found to adopt the anti conformation, while compound **2a** was found in the syn conformation. In the new complex structure of myosin 2 and compound **3**, hydrogen bonds are formed between the hydroxyl group of the phenol ring and Arg428 as well as between the amino group of the pyrrole ring and Lys265 (see Figure 1). At a first glance, the latter interaction appears to be uncommon, as long as both the nitrogen of the pyrrole ring and the amino group of lysine are protonated, making both of them hydrogen donors. However, it is a well-known fact that protein cavities buried inside the macromolecule are often found to exhibit a highly nonpolar character. As can be seen below (see the section Analysis of Pocket Properties) and from Figure 5, the allosteric binding pocket in the myosin motor domain is mainly built by hydrophobic residues, suggesting a nonpolar environment for the binding of pseudilins, in which Lys265 is likely to be deprotonated. The presence of Lys265 in its NH_2 form turns it to a hydrogen acceptor and enables the formation of a hydrogen bond with the NH group of pseudilin's pyrrole ring. Several interactions, both polar and hydrophobic by nature, are found between the halogens of the pseudilin and protein side chains. In contrast to that, Arg428 is not involved in a direct hydrogen bond neither to the hydroxyl group nor to the free amino group in the structures of **2a** and **4a**, respectively. In both of these X-ray structures, Arg428 interacts with the aromatic benzene ring of the pseudilins. Lys265 is in all three cases participating in hydrogen bonding to the OH or NH groups of the compounds and appears to be of high importance. Upon binding, the side chain of Lys265 adjusts its position to facilitate the interaction with the compounds. This becomes obvious upon comparison of the pseudilin complex structures with the wild-type X-ray structure without bound inhibitor in the prepowerstroke state (PDB code: 2JJ9).

Table 1. Inhibition of the Myosin ATPase Activity by the Congeneric Series of Halogenated Pseudilins[a]

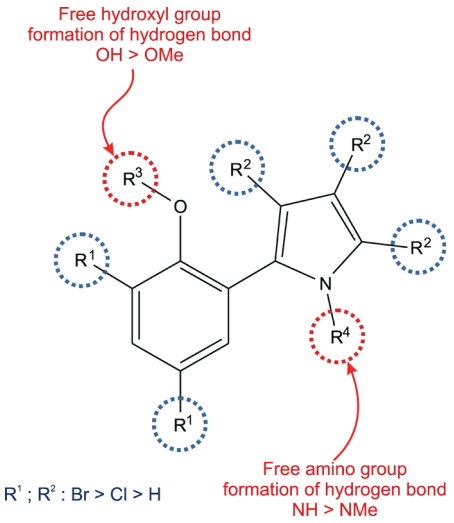

compounds	R^1	R^2	R^3	R^4	IC_{50} (μM)
1a	H	H	H	H	>1 mM
1b	H	H	Me	H	>1 mM
2a	Br	Br	H	H	24.4 ± 1.5
2b	Br	Br	Me	H	91.9 ± 1.2
2c	Br	Br	H	Me	125.4 ± 7.5
2d	H	Br	Me	H	182.2 ± 14.4
3	Cl	Br	H	H	47.2 ± 3.2
4a	Cl	Cl	H	H	126.3 ± 21.0
4b	Cl	Cl	Me	H	274.5 ± 16.5
4c	Cl	H	Me	H	ND
4d	H	Cl	Me	H	ND

[a] ND, not determined due to low solubility.

dx.doi.org/10.1021/jm200259f |*J. Med. Chem.* 2011, 54, 3675–3685

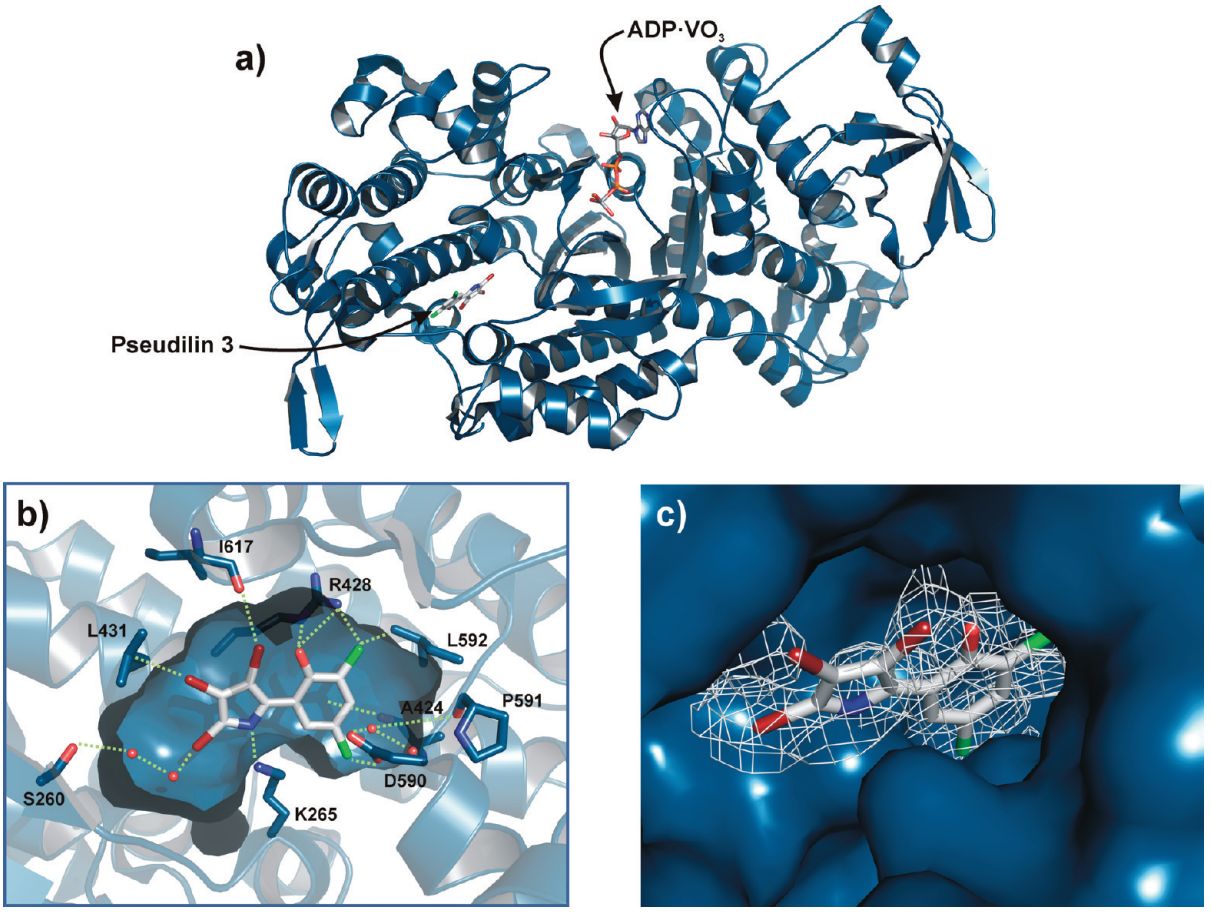

Figure 1. X-ray crystal structure of the *Dd* myosin 2 motor domain in complex with inhibitor **3** and ADP·VO_3. (a) Overview of the refined model of the new X-ray structure in the ribbon representation. The inhibitor and the nucleotide are shown in stick representation. (b) Binding mode and interaction pattern of inhibitor **3** in the binding pocket. (c) Section of the composite $2F_o - F_c$ electron density omit map, contoured at 1.0 σ.

The side chain conformation differs between the structures by up to ~3.2 Å, with a residual root-mean-square deviation (rmsd) of up to 1.04 Å.[2] A further conserved feature of the binding modes of the different pseudilins is the existence of an ordered two water cluster, which mediates the interactions of the inhibitors with the motor protein. These waters are mainly kept in position by Ala420, Asp590, and Pro591. Comparison of the position of the mixed compound **3** and inhibitor **2a** shows a shift of 1.0−1.3 Å for the pyrrole rings, whereas the phenol rings display a shift of ~2.5 Å and are rotated by ~180° against each other. Ligand **4a** is shifted by about 3.0−3.4 Å toward loop 2, as compared to inhibitor **3**, and rotated by approximately 180° (see Figure 2). Several minor adjustments of amino acids in the binding pocket are observed as a result of the complex formation.

SAR. We measured actin-activated ATP turnover by *Dd* myosin 2 to determine the inhibitory activity of the 11 pseudilins (see Table 1). Within the observed range, compounds possessing bromine substituents showed an increased effect over compounds with chlorines. A smaller number of halogen substituents leads to a decrease and finally to a complete loss of activity. Nonhalogenated compounds exhibit no effect at all. The highest inhibitory potency on *Dd* myosin 2 was observed for compound **2a** with an IC_{50} of 24.4 ± 1.5 μM. The transition from penta-brominated to penta-chlorinated pseudilins is associated with an increase in the IC_{50} of more than 5-fold. In comparison, the change of bromine substituents to chlorines only at the phenol ring increases the IC_{50} by a factor of ~2. This fits to the general trend for the influence of the halogen substitution on the inhibitory activity of the pseudilins: bromine (Br) > chlorine (Cl) > hydrogen (H). Methylation of the hydroxyl group of the phenol to the corresponding methyl ether resulted in both cases, fully brominated (**2b**) and chlorinated (**4b**), in a considerable loss in inhibitory potency (3.7- and 2.2-fold). Likewise, the methylation of the amino group of the pyrrole ring of compound **2a** to **2c** reduced the inhibitory potency of the pseudilins ~5-fold. The effect of partial halogenation was estimated with **2d**, where only the pyrrole ring is brominated and amounts to a factor of ~2.0 [ΔIC_{50} (**2d**)/IC_{50} (**2b**)]. The corresponding effect could not be determined for the chloro derivative **4d**, due to solubility limitations. Within the accessible concentration range, compounds **1a** and **1b** do not show any obvious effect at concentrations up to 1 mM, whereas the IC_{50} of **4c** and **4d** could not be determined due to solubility limitations.

Molecular Dynamics. To study the dynamic behavior of the pseudilin inhibitors in fully solvated protein (myosin motor domain, residues 2−755), molecular dynamics (MD) simulations were performed using the Gromacs software suite[6] and the OPLS all-atom force field.[8] Starting coordinates were taken from the three pseudilin−*Dd* myosin 2 motor domain complex X-ray structures by using the crystallographically defined binding poses of **2a** for all brominated pseudilins, **3** for the mixed ligand, and **4a** for all chlorinated inhibitors. The complex structures that were

dx.doi.org/10.1021/jm200259f |*J. Med. Chem.* 2011, 54, 3675–3685

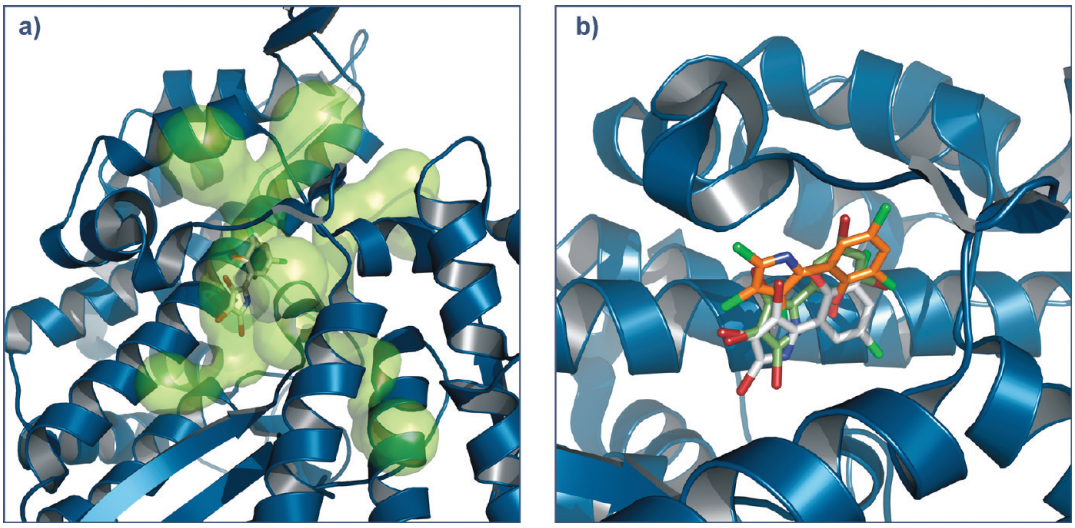

Figure 2. (a) Representation of the various openings and tunnels (lime, transparent surfaces) of the pseudilin binding pocket that leads to the exterior, computed with Caver.[7] (b) The different binding orientations of the pseudilins found in the X-ray crystal structures. Color code of the ligands: carbon: olive = inhibitor **2a**, white = inhibitor **3**, and orange = inhibitor **4a**; nitrogen, blue; oxygen, red; chlorine, green; and bromine, brown.

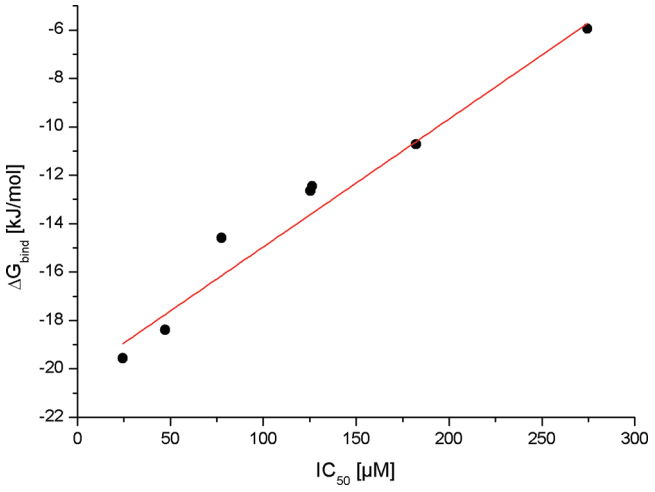

Figure 3. Correlation curve between the experimentally determined inhibitory activities and the binding free energies calculated from the MD simulations.

not crystallographically solved were obtained by in silico replacement of the corresponding ligands. All complexes were energy-minimized and equilibrated. Production runs per complex were performed for 35 ns. To determine the binding affinities of the congeneric series of halogenated pseudilins toward myosin 2 from the MD simulations and to compare the computational results with the experimentally determined IC_{50} values, we calculated the free binding energy ΔG_{bind} using the linear interaction energy (LIE) approach, developed by Åqvist et al.[9] The in silico affinities are in good agreement with the experimental inhibitory activities and validate the accuracy of the MD simulations (see Figure 3 and Table 2).

Analysis of the MD trajectories showed a preference of the nonmethylated pseudilins in the pocket toward the formation of two classical hydrogen bonds to the protein (see Figure 4). Both the free hydroxyl group of the phenol ring and the NH group of the pyrrole ring are involved in hydrogen bonding during the simulations mainly with residues Lys265, Arg428, Asp590, and Ser619. Additionally, transient interaction partners of the pseudilins in the course of the MD simulations include Leu592, Asn616, Ile617, and Arg620. Nevertheless, the compounds seem to retain a high degree of flexibility within the pocket, which could lead to a favorable entropic contribution to the binding free energy. Unfortunately, the total change in entropy upon binding is computationally poorly accessible, and reliable estimations are therefore not available. In addition, the total entropy change is composed of several different contributions, including the expulsion of water molecules from the protein cavity, desolvation of the ligand, changes in the translational, and rotational and internal degrees of freedom of the ligand or of protein residues. Therefore, the total entropy change does not linearly depict the ligand's conformational mobility in the binding pocket. To achieve more insight about the ligand's contributions to the entropy change, we used the quasiharmonic approximation (QH)[10] to calculate configurational entropies from the MD simulations of the ligands in the binding pocket and in solution. In the QH assumption, absolute configurational entropies are calculated from the mass-weighted covariance matrix by applying a one-dimensional quantum-mechanical harmonic oscillator. We computed internal configurational entropy differences of the bound and unbound inhibitors by applying eq 4 on the absolute entropies calculated for the ligands bound to protein and in solution. To remove the overall translational and rotational motion during the entropy calculation, the ligands were superimposed using a least-squares fit with the ligand atom coordinates as references along the trajectory. For all tested compounds, the observed configurational entropy difference was relatively low (20−27 J mol^{-1} K^{-1}). Hence, the compounds do not lose much of their internal degrees of freedom. Moreover, we calculated the absolute entropy of the ligands in the pocket by using the protein coordinates as reference for the least-squares fitting. This was done to account for relative ligand movements in the protein cavity. In all cases, the resulting values are notably higher than the entropies calculated by applying the ligand coordinates to the fitting procedure. The increased absolute entropy values indicate the considerable mobility of the ligands

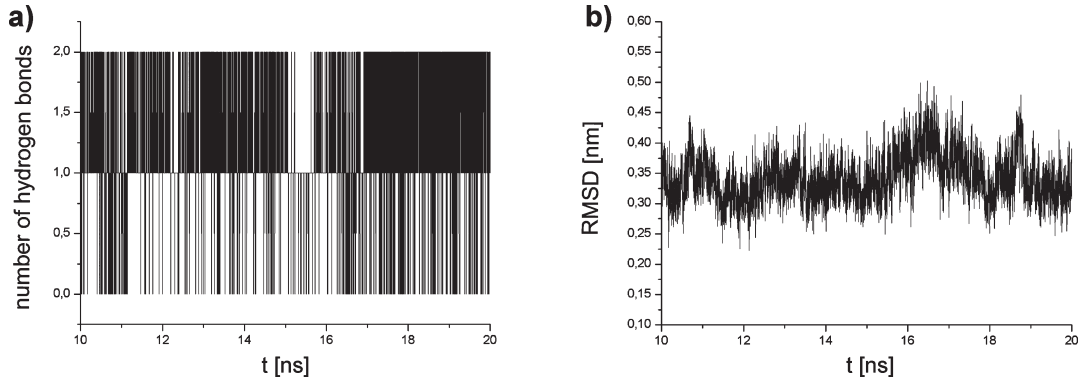

Figure 4. Analysis of the behavior of the pseudilins in the binding pocket during the MD simulations. For clarity, only a 10 ns section of the actual MD simulation is shown. (a) Diagram of the number of hydrogen bonds between the protein and the pseudilin **3** along the MD trajectory. Default cutoff values for the hydrogen bond distance of 3.5 Å and angle cutoff of 30° were used for the determination of the number of hydrogen bonds. (b) rmsd plot of pseudilin **3** in the allosteric pocket during the MD simulation. The atom coordinates of the protein were used for the least-squares fit. Note the fluctuations in the rmsd.

Table 2. Comparison of Experimental Activities and Predicted Binding Free Energies

compound	IC_{50} (μM)	ΔG_{bind} (kJ mol^{-1})
2a	24.4	−19.57
3	47.2	−18.39
2b	77.6	−14.59
2c	125.4	−12.64
4a	126.3	−12.45
2d	182.2	−10.72
4b	274.5	−5.95

Table 3. Configurational Entropies Calculated from the MD Simulations with the QH

	J mol^{-1} K^{-1}			
compound	$S_{complex}$ (ligand)	S_{free} (ligand)	ΔS_{conf}	$S^{transl}_{complex}$ (protein)
2a	209.765	230.545	−20.780	430.281
3	206.273	228.928	−22.655	426.768
4a	201.657	229.049	−27.392	428.094

in the pocket (see Table 3). The occurrence of significant fluctuations in the rmsd plot of the ligand coordinates in the protein provides additional support for the mobility of the ligands in the allosteric pocket (see Figure 4).

Analysis of Pocket Properties. To gain more information about the mechanism of allosteric inhibition by the halogenated pseudilins and to rationalize the affinity and specificity behavior toward certain myosin isoforms, we analyzed the electrostatic and hydrophobic properties of the binding pocket. Solving the Poisson−Boltzmann equation with the adaptive Poisson−Boltzmann solver (APBS),[11] we determined the electrostatics of the crystallographically defined pocket. The inner face of the binding site possesses a number of polar hot spots that are involved in direct hydrogen bonding to the pseudilin inhibitors. However, as can be seen from the hydrophobic surface mapping, there are large clusters of hydrophobic residues or areas that contribute significantly to the binding of the inhibitors and therefore to the unfolding of the inhibitory effect. The halogen substituents of the ligands are accommodated in these large unpolar patches and interact through hydrophobic forces with the protein (see Figure 5).

The comparison of the crystallographic *B* factors of the bound and the unbound form indicates a decrease of the global mobility of the myosin motor domain in the presence of the inhibitors. The quantity of the decrease in protein flexibility correlates with the inhibitory potency of the small molecules (see Figures 6 and 7). Generally, the crystallographic *B* factor indicates the amount of atomic displacement around an average position, thus providing an estimate of the relative mobility of different parts of the protein. Subtracting the normalized *B* factors of the inhibitor-free structure and the particular inhibitor-bound structure shows a global decrease of flexibility or cooling of the majority of the motor domain up to the relay loop region. Figure 7 shows the RMSF values, calculated from the MD trajectories. The amount of reduction in protein fluctuations in the complexes correlates with the inhibitory activity of the bound pseudilin. To validate the results of the MD simulations, *B* factors were calculated from the RMSF values according to $\langle u_k^2 \rangle = (3/8\pi^2)B_k$ and compared to the crystallographic *B* factors (see Figure 7b). The *B* factors from the MD simulations follow the same trend as the experimental values but differ in the size of the fluctuations.

DISCUSSION

Halogenated pseudilins are potent inhibitors of the myosin motor function. While the activity of distinct members of the pseudilins for class 1 and class 5 myosins is in the low micromolar range, the inhibitory potency for myosin 2 is more moderate (tens to hundreds of micromolar). Although the binding site is the same for all pseudilins, the way they are binding varies to some extent. On the one hand, this variation in binding mode is caused by the nature of the different halogen substituents on the pseudilins; on the other hand, the crystallographically determined binding poses represent the energetically favored and therefore dominant ensembles of conformations in the allosteric binding pocket. To probe these assumptions, we carried out classical MD simulations of the complexes in solution. Over the simulation time, the nonmethylated halogenated pseudilins populated preferentially conformations with two intact hydrogen bonds to the myosin motor domain. Thus, both the OH and the

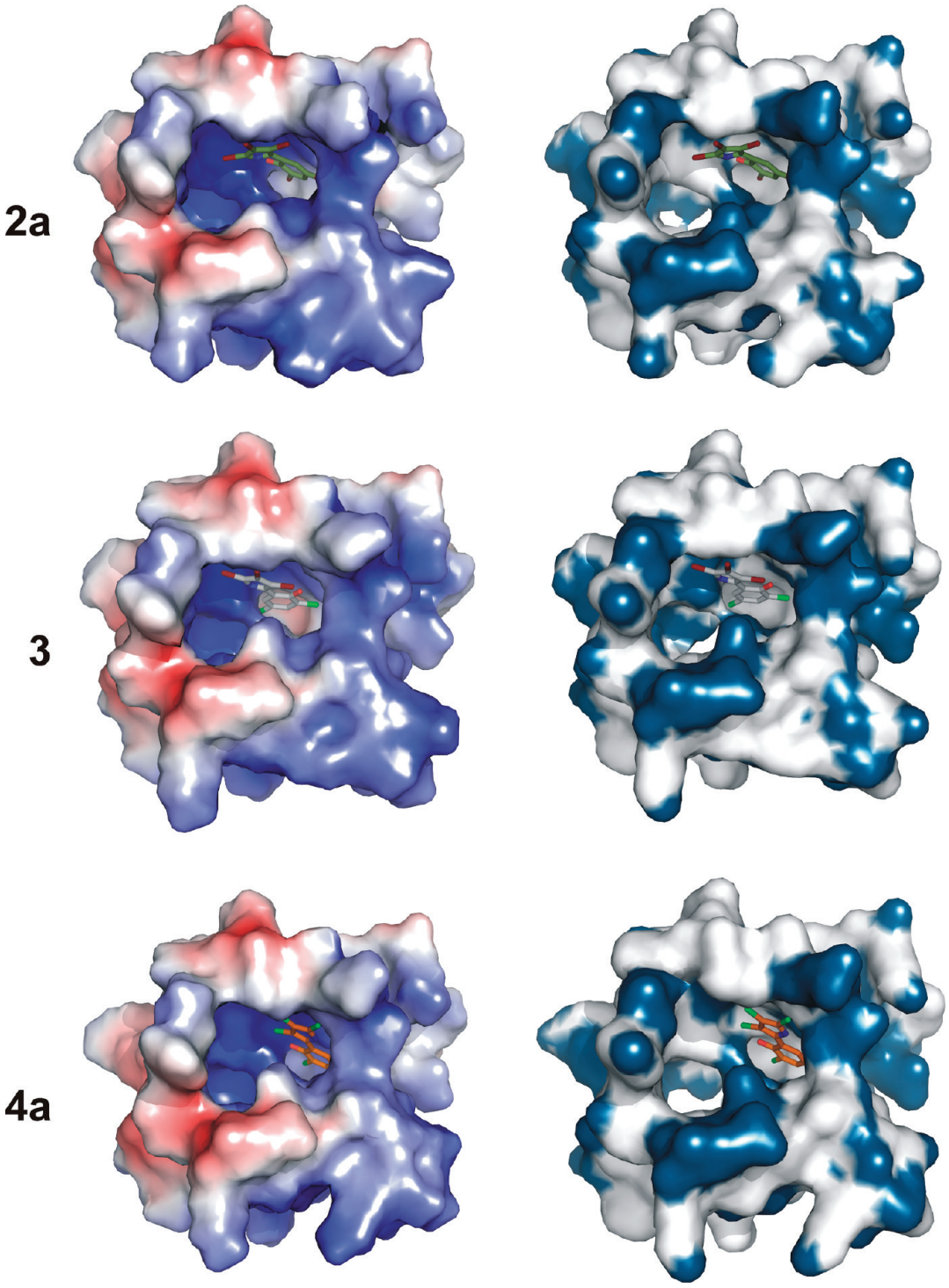

Figure 5. Representation of the properties of the myosin binding pocket. The left column shows the electrostatic potential plotted on the molecular surface of the *Dd* myosin 2 pocket as observed in the crystal structures of the three pseudilin inhibitors. Polar hot spots at the rear and the front right part of the pocket are involved in hydrogen bonding to the pseudilins. The right column shows the hydrophobic surface mapping for the same pockets. Note the hydrophobic patches in the binding cavity and the different accommodation of the halogen substituents for the different pseudilins. Color code: white = hydrophobic, and blue = hydrophilic.

NH groups form hydrogen bonds to the protein, which are important for binding. This observation is supported by the results derived from ATPase activity assays. The inhibitory activity of the pseudilins is considerably reduced, when either the OH or the NH group is methylated. However, these two interacting groups are not the sole determinants for the affinity and inhibitory properties, since nonhalogenated compounds **1a** and **1b** show no activity at all. Number, size, and polarity of the halogen substituents affect the inhibitory potency of the halogenated pseudilins. However, what causes the increased potency of

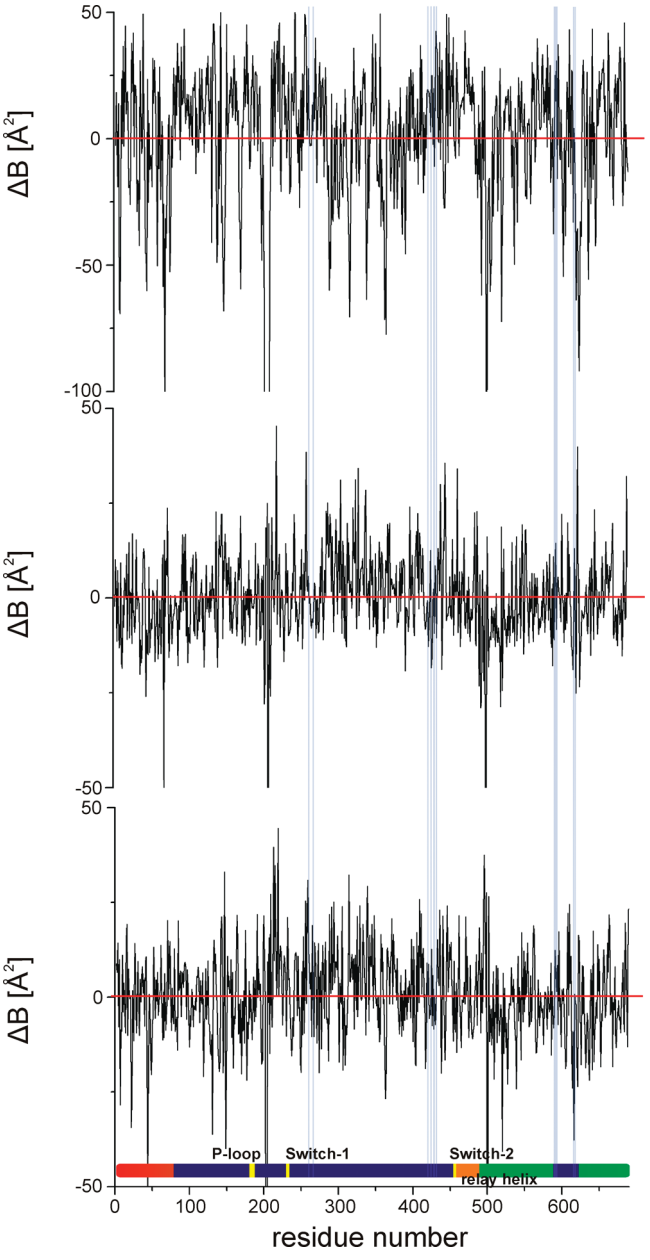

Figure 6. Diagram of the normalized crystallographic *B* factors against the residue number as $\Delta B = B_{\text{unbound}} - B_{\text{bound}}$. 2JJ9 serves as an unbound structure. The graphs show from top to bottom the deviations in the *B* factors for motor domain residues in the presence of **2a** ($\Delta B = B_{2JJ9} - B_{2JHR}$), **3** ($\Delta B = B_{2JJ9} - B_{2XO8}$), and **4a** ($\Delta B = B_{2JJ9} - B_{2XEL}$). Regions of the myosin motor domain are denoted by the color bar at the bottom. The following color code is used: red = N-terminal domain, blue = U50 kDa domain, green = L50 kDa domain, orange = relay helix, and yellow = P loop, switch 1, and switch 2, respectively. Residues interacting with the halogenated pseudilins are indicated by the vertical, transparent blue bars.

compounds possessing bromine rather than chlorine substituents? Analysis of the properties of the binding pocket in *Dd* myosin 2 reveals polar hot spots, which are involved in maintaining the hydrogen bonds to the inhibitors, as well as clusters of hydrophobic residues. These apolar residues interact via multiple hydrophobic interactions mainly with the halogens of the pseudilins. Because bromine is less electronegative than chlorine and the C−Br bond is less polar than the C−Cl bond, stronger hydrophobic interactions can be formed between the bromine substituents and the aliphatic and aromatic side chains of the protein. In addition, the larger size of the bromines facilitates the steric accommodation of the pseudilins in the pocket, as can be seen in the structure of the complex formed by **2a** (see Figure 5). The link between allosteric binding site polarity, affinity, and biological activity of pseudilins with different halogen substituents raises the question about the interaction of halogenated pseudilins with different myosin isoforms. The polarity of the pseudilin binding pocket is increased in most class 1 myosins, due the presence of an increased number of polar and charged amino acids. The inhibitory activity of PClP (**4a**) is significantly enhanced toward class 1 myosins, while **4a** has a low activity toward myosin 2 and 5. In contrast, PBP (**2a**) displays greater inhibitory potency and affinity with myosin 5, which possesses a more hydrophobic allosteric binding site and is less potent in the context of myosin 2 with its moderately hydrophobic pocket. Pseudilin **3** with mixed halogen substitution shows no clear preference for a myosin isoform (see the Supporting Information, Figure 2SI). Therefore, we hypothesize that chlorine-substituted pseudilins are more potent in the context of myosin isoforms with polar allosteric binding pocket, while brominated pseudilins exhibit a greater potency in the context of more hydrophobic binding pockets.

Upon complex formation, ligands usually experience a loss in translational, rotational, and internal degrees of freedom. The loss in internal conformational degrees of freedom of the pseudilins is very low, as computed for the superpositioned inhibitor coordinates along the MD trajectory by means of least-squares fitting. Using the protein atoms for the fitting procedure allows the investigation of the relative movements of the ligand to the protein; therefore, it constitutes a direct means for the description of the translational entropy [$S^{\text{transl}}_{\text{complex}}$ (protein)] of the pseudilin within the protein. The values of the translational entropy are notably higher than the configurational entropies and suggest a significant mobility of the pseudilins in the pocket. Therefore, the results of the MD simulations indicate that the halogenated pseudilins retain some degree of mobility while bound in the allosteric pocket, making a positive entropic contribution to the free energy of binding.

To capture the mode with which these small molecules carry out their inhibitory action is quite challenging, since the X-ray structures of the complexes do not show large differences. Inhibitor binding does not induce movements between protein subdomains. Here, we show that allosteric inhibition by halogenated pseudilins is mediated by the combined effects of global changes in protein dynamics and direct communication between the catalytic and the allosteric sites via a cascade of small conformational changes. The direct signal relay mechanism acts over a distance of ∼19 Å and involves at least seven amino acid residues and two water molecules (see Figure 8). As it is known from most crystal structures of the myosin motor domain in the prepower stroke state, the lytic water molecule (H_2O_{lyt}), which is positioned properly for an in-line attack to the γ-phosphate mimic of the nucleotide analogue, has also been found in the myosin·ADP·VO_3 structure without bound inhibitor (PDB code: 2JJ9). However, this critical water molecule is not preserved in any of the three myosin−inhibitor complex structures.[2] The absence of the lytic water is a consequence of rearrangements in protein side chain orientations along the allosteric path, which is initiated by binding of a halogenated pseudilin to the

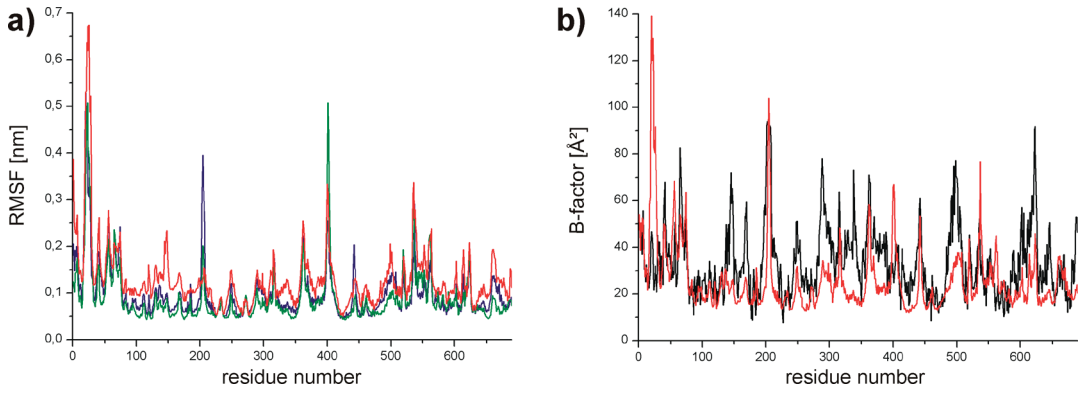

Figure 7. (a) Comparison of the root-mean-square fluctuations (RMSF) of the protein calculated from the MD trajectories. Color code: green = **2a**, blue = **3**, and red = **4a**. The decrease in flexibility correlates with the inhibitory activity. (b) Comparison of the experimental *B* factors (black) and the *B* factor values calculated from RMSF of the MD trajectories (red) per C_α atom in the complex structure with **2a**.

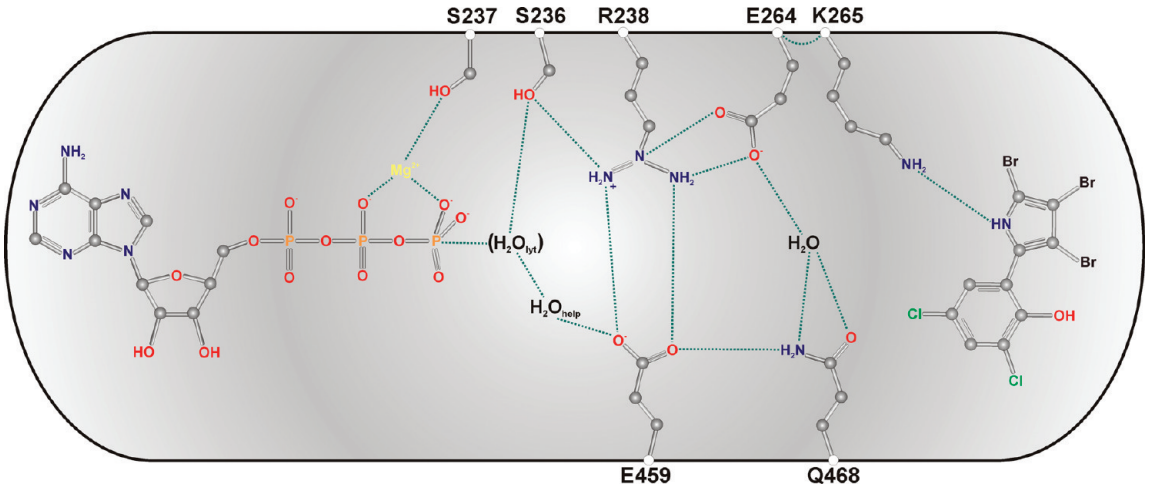

Figure 8. Direct relay path, connecting the allosteric site and the active site via a network of hydrogen bonds. The absence of the lytic water (H_{lyt}) in the inhibitor bound structures is indicated by the parentheses. Note the backbone−backbone hydrogen bond between Lys265 and Arg267, the origin of the relay mechanism. Binding of halogenated pseudilins leads to rearrangements in several amino acid side chains along the path, and as a consequence, it results in the absence of the critical lytic water molecule.

myosin motor domain. Lys265 can be viewed as the starting point for the direct relay mechanism. It is positioned differently in each of the four compared X-ray structures and interacts directly either with the hydroxyl group of the halogenated pseudilins (compounds **2a** and **4a**) or with the amino group of the pyrrole moiety of the inhibitors (compound **3**). Other pronounced changes along the relay path include a slight rearrangement in side chain orientation of Glu264 associated with a shift or complete absence of the hydrogen-bonded water molecule away from the interacting residues (Glu264 and Gln468), as well as movements of the salt bridge residues Arg238 and Glu459 away from each other.

Global communication appears to be most prominent in some of the surface loops but also involves more rigid parts of the motor domain such as the central β-sheet and adjacent helices. *B* factor analysis of the X-ray structures indicates a correlation between the inhibitory potency of the halogenated pseudilins and the extent to which their binding induces global reductions in protein dynamics. Such a decrease of protein flexibility might interfere with the required conformational changes for the motor activity. Myosins pass through a number of different states during their complex motor cycle, and conformational changes are directly coupled to the generation of movement and thereby motor activity. This type of allosteric regulation by small ligand-induced shifts in the population of protein conformer ensembles has been described previously and is generally referred to as "population-shift" model.[12]

CONCLUSIONS

Halogenated pseudilins act as allosteric myosin inhibitors. We have shown that they bind to a site near actin-binding residues at the tip of the myosin motor domain. The inhibitory potency of each compound was investigated by measuring their effect on the turnover of ATP by myosin in the presence of F-actin. Compounds with bromine substituents show an increased inhibitory effect on *Dd* myosin 2 over compounds with chlorine or hydrogen substituents. Analysis of changes in protein structure and dynamics by means of X-ray crystallography and MD simulations revealed the importance of two hydrogen bonds, which are formed between the OH and the NH groups of the inhibitor and polar protein side chains in the binding pocket.

dx.doi.org/10.1021/jm200259f |*J. Med. Chem.* 2011, 54, 3675–3685

Hydrophobic interactions formed between the halogen substituents and the apolar residues in the binding pocket contribute to the binding of the inhibitor. The polarity of the binding pocket in different myosin isoforms and the nature of the halogen substituents of the pseudilins define the specificity of the inhibitors. In addition, calculation of the configurational entropies for the individual halogenated pseudilins indicates a high degree of conformational mobility of the inhibitor in the allosteric pocket, which is supported by the three experimental structures. The extent of loss in configurational entropy is relatively low and therefore contributes positively to the binding affinity. Analysis of the different myosin−inhibitor structures and the structure without bound inhibitor revealed a direct signal relay path that links the allosteric binding site to the active site. Binding of the halogenated pseudilins affects the interaction network along the relay path by side chain rearrangements and results in the absence of the lytic water. Furthermore, the halogenated pseudilins act via the induction of global changes in protein dynamics. Our results show a strong correlation between binding affinity, the extent to which protein dynamics is reduced, and the inhibitory potency of the halogenated pseudilins. The better understanding of the allosteric coupling associated with the binding of small molecule effectors to myosin enables us to rationalize and streamline the process of developing more potent and selective myosin inhibitors for therapeutic applications.

EXPERIMENTAL SECTION

Protein Preparation. His_7-tagged motor domain constructs of *Dd* myosin 2 comprising amino acids 1−761 were purified using Ni^{2+}-chelate affinity chromatography.[13] Rabbit F-actin has been prepared as described elsewhere.[14]

Synthesis of the Small Molecule Inhibitors. The synthesis of the halogenated pseudilin derivatives using a silver(I)-catalyzed cyclization reaction has been described elsewhere.[5]

Crystallization, Data Collection, and Refinement. Crystals of the protein−ligand complex were obtained by cocrystallization of the purified *Dd* myosin 2 motor domain (M761-SSB), fused to a N-terminal His_7 tag and a C-terminal SSB tag,[15] with a final concentration of 1 mM 2,4-dichloro-6-(3,4,5-tribromo-1*H*-pyrrole-2-yl)phenol, 1 mM ADP, and 1 mM sodium *meta*-vanadate at 4 °C by vapor diffusion using the hanging-drop geometry. The mixture was incubated on ice for 1 h and subsequently mixed with an equal volume of reservoir solution containing 50 mM HEPES (pH 6.8), 110 mM NaCl, 11% PEG_{MME} 5000, 2% MPD, 5 mM $MgCl_2$, 5 mM DTT, and 1 mM EGTA. Prior to data collection, the crystals were transferred to a cryoprotection solution containing reservoir solution mixed with additional 25% ethylene glycol and flash-cooled in liquid nitrogen. Diffraction data were collected at EMBL beamline X13, DESY, Hamburg. Integration and scaling of the data were done using the program XDS.[16] Molecular replacement using PDB 2JJ9 as a starting model and model refinement were performed using CNS 1.2[17] and Phenix 1.6.[18] A random 5% of the data was excluded for cross-validation. Model building and validation were carried out using COOT.[19] The coordinates were stored in the protein database,[20] identification code: 2XO8.

Steady-State ATPase Measurements. Actin-activated steady-state ATPase experiments were performed following the absorbance change during NADH oxidation in a PK/LDH-coupled ATPase assay at 340 nm excitation. The assay was performed at 25 °C in a buffer containing 25 mM Hepes, 25 mM KCl, and 4 mM MgCl2. Myosin constructs were added to a cuvette containing 0.5 mM DTT, 0.5 mM ATP, 0.2 mM NADH, 0.5 mM phosphoenolpyruvate (PEP), 0.02 mg/mL lactate dehydrogenase (LDH), 0.05 mg/mL pyruvate kinase (PK), and 30 μM F-actin.

MD Simulation. All MD simulations were carried out with the Gromacs 4.0 software package and the OPLS all-atom force field. For the brominated pseudilins, we used the PBP (**2a**)−*Dd* myosin 2 structure (2JHR) as the starting coordinates and exchanged **2a** by the corresponding brominated pseudilins. In the case of the mixed pseudilin TBDClP (**3**), the newly solved X-ray structure (2XO8) was used, and for the chlorinated derivatives, the PClP (**4a**) structure (2XEL) served as the starting structure. The structures were truncated after residue 755, before applying to MD simulations. Atomic charges were taken from the force field. Missing force constants for the bond stretching and angle bending of the Br−C and Cl−C bonds in the inhibitors were derived from the compatible general Amber force field (GAFF).[21] This exchange of force constants between the two different force fields in this case is possible, since both force fields use the harmonic oscillator to describe the bond and angle energy terms. Thus, they both have the same functional form. In addition, derivation of the force constants for bond stretching and angle bending in the OPLS all-atom and the GAFF force field origin from the same source, they are either taken from the AMBER force field[22] or optimized to fit quantum mechanical calculations.[8,21,23] All simulations were performed in explicit solvent using the TIP4P water model[24] in a *NpT* ensemble at 300 K and 1 bar using Berendsen temperature coupling and Parrinello-Rahman pressure coupling. Long-range electrostatics were treated with particle-mesh Ewald[25] with a grid spacing of 0.12 nm and an interpolation order of 4, while short-range Van der Waals and Coulomb forces were treated with a 14 and 10 Å cutoff, respectively. We used a 2 fs time step during the production runs and constrained all bond lengths with the LINCS algorithm.[26] After initial energy minimization with the steepest descent algorithm to a force of 1000 kJ mol^{-1} nm^{-1}, the coordinates were optimized with the conjugate gradient algorithm to a final force of <10 kJ mol^{-1} nm^{-1}. The solvent molecules were equilibrated for 100 ps. Subsequently, MD simulations for 40 ns were performed. Within the first 5 ns of MD simulations, the backbone rmsd of the protein converged toward a plateau. This 5 ns equilibration period was omitted from further investigations, and only the last 35 ns was used for analysis.

To compute the binding free energy (ΔG_{bind}), we used the LIE method. In the LIE formulation, the free energy of binding is computed through evaluating the nonbonded energy terms, van der Waals, and electrostatic terms of the ligand in complex with the target protein (bound) or in solution (free) along the simulation trajectory, as:

$$\Delta G_{bind} = \alpha\left(\langle V^{vdW}_{l-s}\rangle_{bound} - \langle V^{vdW}_{l-s}\rangle_{free}\right) + \beta\left(\langle V^{el}_{l-s}\rangle_{bound} - \langle V^{el}_{l-s}\rangle_{free}\right) \quad (1)$$

We used the scaling factors $\alpha = 0.18$ and $\beta = 0.50$ for the calculation of the pseudilin binding free energies.

Configurational entropy estimates were computed with the QH. The QH approximation was shown to be applicable for the calculation of configurational entropies from MD trajectories.[27] Quasiharmonic frequencies ω_i were calculated from the eigenvalues λ^i of the diagonalized mass-weighted covariance matrix σ', as:

$$\omega_i = \sqrt{\frac{kT}{\lambda_i}} \quad (2)$$

We computed the absolute configurational entropy using the equation:

$$S_{ho} = k\sum_{i}^{3n-6}\frac{\hbar\omega_i/kT}{e^{\hbar\omega_i/kT}-1} - \ln\left(1-e^{-\hbar\omega_i/kT}\right) \quad (3)$$

To estimate the differences in internal configurational entropy upon binding of the halogenated pseudilins to the myosin motor domain, we

performed independent simulations of the compounds in solution and in the protein cavity. The inhibitor atoms were used for the least-squares fitting procedure of the snapshots along the MD trajectory during the entropy calculation, thereby removing overall rotation and translation. The differences in configurational entropy were calculated, as:

$$\Delta S_{conf} = S_{complex}\ (\text{ligand}) - S_{free}\ (\text{ligand}) \quad (4)$$

Repeating the entropy calculation of the ligand in complex with myosin, while using the atoms of the protein for the least-squares fit, the resulting entropies account additionally for the translation of the compounds in the binding pocket.

■ ASSOCIATED CONTENT

Supporting Information. Summary of data collection and refinement statistics, schematic interaction plots for the three X-ray structures of the myosin 2−pseudilin complexes, inhibition of the actin-activated ATPase activity of different myosin isoforms by TBDClP (**3**) at different concentrations, and sections of the $2F_o - F_c$ electron density omit maps of the *Dd* myosin 2 active sites showing that binding of a pseudilin results in the absence of the lytic water through the allosteric relay path. This material is available free of charge via the Internet at http://pubs.acs.org.

Accession Codes

The PDB code for the X-ray structure of the *Dd* myosin 2 motor domain in complex with inhibitor **3** is 2XO8.

■ AUTHOR INFORMATION

Corresponding Author

*Tel: +49-511-532-3700. Fax: +49-511-532-5966. E-mail: manstein.dietmar@mh-hannover.de.

■ ACKNOWLEDGMENT

We thank Roman Fedorov for help and discussions and Petra Baruch for technical assistance. We are grateful to the staff of beamline X13 at the DORIS storage ring of DESY for their support. The work was supported by grant MA 1081/16-1 from the DFG and the Cluster of Excellence "Rebirth" (D.J.M.).

■ ABBREVIATIONS USED

PBP, pentabromopseudilin; PClP, pentachloropseudilin; TBDClP, tribromodichloropseudilin; *Dd*, *Dictyostelium discoideum*; IC_{50}, half maximal inhibitory concentration; SAR, structure−activity relationship; rmsd, root-mean-square deviation; LIE, linear interaction energy; MD, molecular dynamics; ND, not determined; QH, quasiharmonic approximation

■ REFERENCES

(1) Fedorov, R.; Böhl, M.; Tsiavaliaris, G.; Hartmann, F. K.; Taft, M. H.; Baruch, P.; Brenner, B.; Martin, R.; Knölker, H. J.; Gutzeit, H. O.; Manstein, D. J. The mechanism of pentabromopseudilin inhibition of myosin motor activity. *Nat. Struct. Mol. Biol.* **2009**, *16* (1), 80–88.

(2) Chinthalapudi, K.; Taft, M.; René, M.; Heissler, S. M.; Preller, M.; Hartmann, F. K.; Kendrick-Jones, J.; Tsiavaliaris, G.; Gutzeit, H. O.; Fedorov, R.; Buss, F.; Knölker, H.-J.; Coluccio, L. M.; Manstein, D. J., unpublished results.

(3) (a) Ohri, R. V.; Radosevich, A. T.; Hrovat, K. J.; Musich, C.; Huang, D.; Holman, T. R.; Toste, F. D. A Re(V)-catalyzed C-N bond-forming route to human lipoxygenase inhibitors. *Org. Lett.* **2005**, *7* (12), 2501–2504. (b) Burkholder, P. R.; Pfister, R. M.; Leitz, F. H. Production of a pyrrole antibiotic by a marine bacterium. *Appl. Microbiol.* **1966**, *14* (4), 649–653. (c) Laatsch, H.; Renneberg, B.; Hanefeld, U.; Kellner, M.; Pudleiner, H.; Hamprecht, G.; Kraemer, H. P.; Anke, H. Structure-activity relationships of phenyl- and benzoylpyrroles. *Chem. Pharm. Bull.* **1995**, *43* (4), 537–546.

(4) (a) Hanessian, S.; Kaltenbronn, J. S. Synthesis of a Bromine-Rich Marine Antibiotic. *J. Am. Chem. Soc.* **1966**, *88* (19), 4509–4510. (b) Laatsch, H.; Pudleiner, H. Marine Bakterien, I. Synthese von Pentabrompseudilin, einem cytotoxischen Phenylpyrrol aus *Alteromonas luteo-violaceus*. *Liebigs Ann. Chem.* **1989**, *1989* (9), 863–881. (c) Xu, Z.; Lu, X. A Novel [3 + 2] Cycloaddition Approach to Nitrogen Heterocycles via Phosphine-Catalyzed Reactions of 2,3-Butadienoates or 2-Butynoates and Dimethyl Acetylenedicarboxylate with Imines: A Convenient Synthesis of Pentabromopseudilin. *J. Org. Chem.* **1998**, *63* (15), 5031–5041.

(5) Martin, R.; Jäger, A.; Böhl, M.; Richter, S.; Fedorov, R.; Manstein, D. J.; Gutzeit, H. O.; Knölker, H. J. Total synthesis of pentabromo- and pentachloropseudilin, and synthetic analogues—Allosteric inhibitors of myosin ATPase. *Angew. Chem., Int. Ed. Engl.* **2009**, *48* (43), 8042–8046.

(6) Hess, B.; Kutzner, C.; van der Spoel, D.; Lindahl, E. GROMACS 4: Algorithms for Highly Efficient, Load-Balanced, and Scalable Molecular Simulation. *J. Chem. Theory Comput.* **2008**, *4* (3), 435–447.

(7) Petrek, M.; Otyepka, M.; Banas, P.; Kosinova, P.; Koca, J.; Damborsky, J. CAVER: a new tool to explore routes from protein clefts, pockets and cavities. *BMC Bioinformatics* **2006**, *7*, 316.

(8) Jorgensen, W. L.; Maxwell, D. S.; Tirado-Rives, J. Development and Testing of the OPLS All-Atom Force Field on Conformational Energetics and Properties of Organic Liquids. *J. Am. Chem. Soc.* **1996**, *118* (45), 11225–11236.

(9) (a) Aqvist, J.; Medina, C.; Samuelsson, J. E. A new method for predicting binding affinity in computer-aided drug design. *Protein Eng.* **1994**, *7* (3), 385–391. (b) Aqvist, J.; Marelius, J. The linear interaction energy method for predicting ligand binding free energies. *Comb. Chem. High Throughput Screening* **2001**, *4* (8), 613–626.

(10) Karplus, M.; Kushick, J. N. Method for estimating the configurational entropy of macromolecules. *Macromolecules* **1981**, *14* (2), 325–332.

(11) Baker, N. A.; Sept, D.; Joseph, S.; Holst, M. J.; McCammon, J. A. Electrostatics of nanosystems: Application to microtubules and the ribosome. *Proc. Natl. Acad. Sci. U.S.A.* **2001**, *98* (18), 10037–10041.

(12) (a) Laskowski, R. A.; Gerick, F.; Thornton, J. M. The structural basis of allosteric regulation in proteins. *FEBS Lett.* **2009**, *583* (11), 1692–1698. (b) Goodey, N. M.; Benkovic, S. J. Allosteric regulation and catalysis emerge via a common route. *Nat. Chem. Biol.* **2008**, *4* (8), 474–482. (c) Cui, Q.; Karplus, M. Allostery and cooperativity revisited. *Protein Sci.* **2008**, *17* (8), 1295–1307. (d) Tsai, C. J.; del Sol, A.; Nussinov, R. Allostery: Absence of a change in shape does not imply that allostery is not at play. *J. Mol. Biol.* **2008**, *378* (1), 1–11.

(13) Manstein, D. J.; Hunt, D. M. Overexpression of myosin motor domains in *Dictyostelium*: Screening of transformants and purification of the affinity tagged protein. *J. Muscle Res. Cell Motil.* **1995**, *16* (3), 325–332.

(14) Lehrer, S. S.; Kerwar, G. Intrinsic fluorescence of actin. *Biochemistry* **1972**, *11* (7), 1211–1217.

(15) Fedorov, R.; Witte, G.; Urbanke, C.; Manstein, D. J.; Curth, U. 3D structure of Thermus aquaticus single-stranded DNA-binding protein gives insight into the functioning of SSB proteins. *Nucleic Acids Res.* **2006**, *34* (22), 6708–6717.

(16) Kabsch, W. Automatic processing of rotation diffraction data from crystals of initially unknown symmetry and cell constants. *J. Appl. Crystallogr.* **1993**, *26* (6), 795–800.

(17) (a) Brunger, A. T.; Adams, P. D.; Clore, G. M.; DeLano, W. L.; Gros, P.; Grosse-Kunstleve, R. W.; Jiang, J. S.; Kuszewski, J.; Nilges, M.; Pannu, N. S.; Read, R. J.; Rice, L. M.; Simonson, T.; Warren, G. L. Crystallography & NMR system: A new software suite for macromolecular structure determination. *Acta Crystallogr., Sect. D: Biol. Crystallogr.* **1998**, *54* (Part 5), 905–921. (b) Brunger, A. T. Version 1.2 of the

Crystallography and NMR system. *Nat. Protoc.* **2007**, *2* (11), 2728–2733.

(18) Adams, P. D.; Afonine, P. V.; Bunkoczi, G.; Chen, V. B.; Davis, I. W.; Echols, N.; Headd, J. J.; Hung, L. W.; Kapral, G. J.; Grosse-Kunstleve, R. W.; McCoy, A. J.; Moriarty, N. W.; Oeffner, R.; Read, R. J.; Richardson, D. C.; Richardson, J. S.; Terwilliger, T. C.; Zwart, P. H. PHENIX: A comprehensive Python-based system for macromolecular structure solution. *Acta Crystallogr., Sect. D: Biol. Crystallogr.* **2010**, *66* (Part 2), 213–221.

(19) Emsley, P.; Lohkamp, B.; Scott, W. G.; Cowtan, K. Features and development of Coot. *Acta Crystallogr., Sect. D: Biol. Crystallogr.* **2010**, *66* (Part 4), 486–501.

(20) Berman, H. M.; Westbrook, J.; Feng, Z.; Gilliland, G.; Bhat, T. N.; Weissig, H.; Shindyalov, I. N.; Bourne, P. E. The Protein Data Bank. *Nucleic Acids Res.* **2000**, *28* (1), 235–242.

(21) Wang, J.; Wolf, R. M.; Caldwell, J. W.; Kollman, P. A.; Case, D. A. Development and testing of a general amber force field. *J. Comput. Chem.* **2004**, *25* (9), 1157–1174.

(22) Cornell, W. D.; Cieplak, P.; Bayly, C. I.; Gould, I. R.; Merz, K. M.; Ferguson, D. M.; Spellmeyer, D. C.; Fox, T.; Caldwell, J. W.; Kollman, P. A. A Second Generation Force Field for the Simulation of Proteins, Nucleic Acids, and Organic Molecules. *J. Am. Chem. Soc.* **1995**, *117* (19), 5179–5197.

(23) Kaminski, G. A.; Friesner, R. A.; Tirado-Rives, J.; Jorgensen, W. L. Evaluation and Reparametrization of the OPLS-AA Force Field for Proteins via Comparison with Accurate Quantum Chemical Calculations on Peptides. *J. Phys. Chem. B* **2001**, *105* (28), 6474–6487.

(24) Jorgensen, W. L.; Chandrasekhar, J.; Madura, J. D.; Impey, R. W.; Klein, M. L. Comparison of simple potential functions for simulating liquid water. *J. Chem. Phys.* **1983**, *79* (2), 926–935.

(25) Darden, T.; York, D.; Pedersen, L. Particle mesh Ewald: An N log(N) method for Ewald sums in large systems. *J. Chem. Phys.* **1993**, *98* (12), 10089–10092.

(26) Hess, B.; Bekker, H.; Berendsen, H. J. C.; Fraaije, J. G. E. M. LINCS: A linear constraint solver for molecular simulations. *J. Comput. Chem.* **1997**, *18* (12), 1463–1472.

(27) (a) Chang, C.-E.; Chen, W.; Gilson, M. K. Evaluating the Accuracy of the Quasiharmonic Approximation. *J. Chem. Theory Comput.* **2005**, *1* (5), 1017–1028. (b) Carlsson, J.; Aqvist, J. Absolute and Relative Entropies from Computer Simulation with Applications to Ligand Binding. *J. Phys. Chem. B* **2005**, *109* (13), 6448–6456. (c) Baron, R.; van Gunsteren, W. F.; Hünenberger, P. H. Estimating the configurational entropy from molecular dynamics simulations: anharmonicity and correlation corrections to the quasi-harmonic approximation. *Trends Chem. Phys.* **2006**, *11*, 87–122.